Chapter 9

Differential Cross-sections

9.1 Definition and calculation

Perturbative QCD, in addition to providing a prediction of the production cross-section of $c\bar{c}$ pairs in hadronic collisions, can be used to calculate the momentum distribution of these charm quarks.[1] This distribution is a scalar function of momentum, where the domain in momentum space is limited by kinematic constraints to a sphere of radius p_{max}.[2] Integration of the distribution function over this volume V_{int} yields a value equal to the total cross-section:

$$\sigma = \oint_{V_{int}} \frac{d^3\sigma}{d^3p}\, dV = \int_0^{2\pi} \int_0^{p_{max}} \int_{-p_{max}}^{p_{max}} \frac{d^3\sigma}{dp_L\, dp_T\, d\phi}\, dp_L\, dp_T\, d\phi, \qquad (9.1)$$

where p_L is the longitudinal component of the momentum (parallel to the beam axis), p_T is the transverse component, and ϕ is the azimuthal angle about the beam axis. Neither the beam nor the target in E769 is polarized; the absence of any preferred direction which can break the azimuthal symmetry about the beam axis allows us integrate away the ϕ dependence without loss of generality. Further transforming

[1] Here, "charm quarks" is meant to include both quarks and antiquarks. Interestingly, QCD predicts a tiny difference in the c and $\bar{c}$ momentum distributions [37]. In this analysis, we measure the particle-plus-antiparticle differential cross-sections of a given charm meson; therefore we probe indirectly the *average* of the charm quark and antiquark distributions.

[2] As implied by the spherical shape, we are defining momentum in the center-of-mass frame of the interaction. Therefore, p_{max} is given by $E_{CM}/2$ ($\simeq$ 10.8 GeV for E769).

variables, we obtain

$$\sigma = \int_0^{p_{max}} \int_{-p_{max}}^{p_{max}} \frac{d^2\sigma}{dp_L\, dp_T}\, dp_L\, dp_T = \int_0^{p_{max}^2} \int_{-1}^{1} \frac{d^2\sigma}{dx_F\, dp_T^2}\, dx_F\, dp_T^2. \qquad (9.2)$$

Use of the Feynman-x variable facilitates comparison of longitudinal distributions obtained at different energies; such comparisons test the zeroth-order scale invariance expected from the constituent parton model. Via the change from p_T to p_T^2, we obtain a transverse momentum distribution with a simple form which does not vanish at zero.

The bivariate distribution $\frac{d^2\sigma}{dx_F\, dp_T^2}(x_F, p_T^2)$ cannot be factored into a product of x_F and p_T^2-independent parts. Given the level of precision afforded by our data (not to mention the current state of theory), no valuable information is sacrificed by treating the two momentum components separately. We therefore confine our study to measurements of the differential cross-section distributions in each variable, integrated over the other variable:

$$\frac{d\sigma}{dx_F}(x_F) = \int_0^{p_{max}^2} \frac{d^2\sigma}{dx_F\, dp_T^2}(x_F, p_T^2)\, dp_T^2 \qquad (9.3)$$

$$\left.\frac{d\sigma}{dp_T^2}(p_T^2)\right|_{x_F>0} = \int_0^1 \frac{d^2\sigma}{dx_F\, dp_T^2}(x_F, p_T^2)\, dx_F. \qquad (9.4)$$

Note that this definition of the transverse distribution will apply in all that follows, even when the label "$x_F > 0$" is dropped. The extension of the above discussion to differential cross-section distributions for charm mesons is straightforward: the momentum of the quark is simply replaced by the momentum of the hadron containing the quark. Issues surrounding the expected relationship between the quark and hadron distributions are discussed in Chapter 2.

In practice, we measure the $d\sigma/dx_F$ and $d\sigma/dp_T^2$ distributions by obtaining approximate[3] samples of them at a number of points. In order to illustrate the procedure, we use the longitudinal differential cross-section of D meson production, where B represents the beam particle:

[3]Given the bin sizes used in this analysis, the errors associated with this approximation are negligible.

$$\frac{d\sigma}{dx_F}(BN \to DX;\, x_{F(i)}) \simeq \frac{1}{\Delta_i} \int_{x_{F(i)}-\Delta_i/2}^{x_{F(i)}+\Delta_i/2} \frac{d\sigma}{dx'_F}\, dx'_F = \frac{N_{prod}(B, D;\, x_{F(i)})}{F(B)\, T_N}. \quad (9.5)$$

In this equation, $x_{F(i)}$ (Δ_i) is the central value (width[4]) of the ith x_F bin, $N_{prod}(x_{F(i)})$ is the number of D's produced ($|x_F - x_{F(i)}| < \Delta_i/2$) through B-target collisions, and $F(B)$ and T_N appear in the analogous absolute cross-section equation (Equation 8.4).

By binning all $x_F(p_T^2)$-dependent quantities, the calculation of $d\sigma/dx_F$ ($d\sigma/dp_T^2$) in each bin can be carried out exactly as that outlined in Section 8.1.[5] It is easier, however, to discard temporarily all quantities which do not depend on x_F (p_T^2), calculate the shape of the differential distribution, and then fix the normalization so that following equations holds:

$$\sigma(BN \to DX)_{x_F>0} = \sum_i^{x_F>0} \frac{d\sigma}{dx_F}(BN \to DX;\, x_{F(i)})\, \Delta_i \quad (9.6)$$

$$= \sum_j \frac{d\sigma}{dp_T^2}(BN \to DX;\, p_{T(j)}^2)\, \Delta_j, \quad (9.7)$$

where the sum i (j) runs over x_F (p_T^2) bins for which there is data.

Dropping the subscript which indicates the binning of the kinematic variables, it is now sufficient to write

$$\frac{d\sigma}{dx_F}(BN \to DX;\, x_F) \propto \frac{N_{obs}(B, T, D \to xyz;\, x_F)}{Acc(T, D \to xyz;\, x_F)}$$

$$= \frac{N_{obs}(B, T, D \to xyz;\, x_F)\; N_{gen}^{MC}(D \to xyz;\, x_F)}{\hat{N}_{obs}^{MC}(T, D \to xyz;\, x_F)}. \quad (9.8)$$

See the text immediately following Equation 7.1 or 8.14 for the definitions of these quantities. Note that the MC weighting used to obtain $\hat{N}_{obs}^{MC}$ differs in the absolute

[4]The x_F bins have a constant width of 0.1, but as explained in Section 6.3.2, the width of a p_T^2 bin is either 1 or 2 GeV^2.

[5]This binning procedure rests on the assumption that measurement resolutions for x_F and p_T^2 are small compared to the relevant bin width. This assumption is supported by MC studies, which indicate that typical measurement errors associated with these variables are on order of 10% of the bin width used.

and differential cross-section analyses; these differences are detailed in Section 7.1. An equation analogous to (9.8) holds for $d\sigma/dp_T^2$.

In Section 9.3.1, combined D differential cross-section results ($d\sigma/dx_F$ and $d\sigma/dp_T^2$) for combined π, combined K, and p beams are tabulated. In addition, for those (combined or individual) charm species/beam combinations for which the differential distributions are well-measured, plots showing fits to standard parametrizations are provided.

9.2 Systematic errors

The conclusion of this section will be that systematic errors on the shapes[6] of the differential cross-section distributions are negligible compared to their statistical counterparts. Despite the caveats placed on the interpretation of the standard shape parameters as fundamental physical quantities (see Section 9.3.1), nevertheless they remain our most useful handle on variation in the shapes of $d\sigma/dx_F$ and $d\sigma/dp_T^2$ due to any given change in assumptions or analysis procedure.

Distributions in x_F (p_T^2) are generally well-fit by functions with one (one or two) shape parameters, namely n (b or α and β); the specific forms of these functions, the quality of given fits, and the values of parameters returned by these fits are discussed in detail in Section 9.3.1. For our present purpose, we need only know the scales of the typical statistical errors in these parameters so that we may judge whether a given systematic error contributes appreciably when combined in quadrature. For our highest-statistics sample (combined π beam, combined D), n is measured to a relative precision of 4.4%, b to 4.6%, α to 21%, and β to 12%.

Information concerning systematic dependencies of D meson differential distribution shapes can be found in the extensive previous studies carried out by members of the E769 collaboration. Two E769 papers reporting differential cross-section results have been published. The first ([6]) is on π^--induced production of D^+ and D^0, the second ([9]) on $\pi^\pm$-induced production of D^{*+}. We will concern ourselves with the

[6]Because these distributions are presented with absolute normalization, the systematic errors detailed in Section 8.2 apply. However, in this chapter we concern ourselves only with the shapes of the distributions, which are in general much less sensitive to these effects.

former (including supporting studies found in the theses of E769 graduate students [41, 43]); due to the relatively-low statistics of the D^* signal used in this analysis, statistical errors are sure to swamp any systematic effects connected specifically to this species.

In the pseudoscalar D paper, systematic errors in the differential acceptances are said to "include the uncertainties in trigger simulation and detector efficiencies" and to be "small compared to the statistical errors in the data"; only these latter errors on the shape parameters are quoted. These statements are supported by the systematic error studies detailed in Section 6.6 of S. Takach's thesis (from which the results of the aforementioned paper are taken) ([41], pp.115-118). He finds the relative errors in n and b due to uncertainties in the MC weighting (Čerenkov and trigger efficiency) to be on the order of 1%. He also confirms that weighting to correct for the production distributions generated by the MC (a correction used in the present analysis only for absolute cross-section calculations) has a negligible impact on the shape parameters. In addition to these systematic errors, Takach estimates the error due to the procedure used to fit the mass plots. As this error is correlated to the dominant statistical error (which was larger for his results), we assess the importance of the former based on its ratio of the latter. This ratio is less than 0.5, indicating that any systematic component independent of the statistical error will be small.

One potentially significant systematic error in the differential acceptance which is not addressed in Takach's thesis is that associated with DC efficiencies, specifically uncertainty in the measured dimensions of the "DC holes", areas of diminished efficiency near the beam line. In Section 6.3 of his thesis on x_F-dependence in π^--induced D^+ production ([43], pp.94-95), Z. Wu provides some relevant information. In bins of x_F, he shows the average effect on acceptance due to $\pm 1\sigma$ variations in the widths of the DC holes. At higher values of x_F, the relative change in the acceptance is at most a few percent more than the effect in the x_F range where most of the data resides. Since only *differences* in the relative changes in acceptance at low and high x_F can effect the shape of the differential acceptance, this contribution to the systematic error must be negligible. In fact, the error is even much lower than the above discussion might imply, because the changes in acceptance obtained by varying

all DC hole widths together (by $\pm 1\sigma$) is a gross overestimate of the systematic error which should properly be associated with the independent uncertainties in the DC hole dimensions.

In the present analysis, combined D differential cross-sections are used to estimate systematic relative errors on the shape parameters. As discussed in Section 9.3.1, the standard n (b) parameter exhibits a systematic dependence on the upper (lower) limit chosen for the fit range. Rather than serving as evidence of systematic errors in well-defined fundamental quantities, this range dependence points to the inadequacy of these one-parameter functions as analytic forms for the differential distributions. Therefore, no systematic error is associated with n and b due to this effect; rather, these quantities are reported as range-dependent.

Fits to $d\sigma/dx_F$ and $d\sigma/dp_T^2$ also show some sensitivity to the choice made in the point at which to exclude bins for which the data signal was not well-measured. By adding an extra bin (at high x_F or p_T^2) to the number indicated by the default cutoff in signal significance (described in Section 9.3.1), this systematic error was estimated and found in all cases to be a fraction of the statistical error. As these errors are correlated, any independent systematic effect is even less significant and therefore negligible.

One final systematic error, applying to the combined D differential cross-section results, arises from the relative weights given D^+, D^0, and D_s acceptances in the composite average acceptance. These weights are calculated in Section 7.2.6. An overestimate of this error was obtained by varying the $D^+/D^0/D_s$ cross-section ratio assumed from 2:4:1 to 2:2:1; this changes n by about 30% of the statistical error. As shown in Figs. 7.11 and 7.12, differential acceptance shapes are insensitive to the identity of the D meson.

9.3 Results

9.3.1 Differential cross-sections

Combined D differential cross-section results for π, K, and p beams are given in Tables 9.1 and 9.2. While these and other results presented in this section are absolutely normalized using the results of Chapter 8, what shall concern us here are the *shapes* of these differential distributions. Differential cross-section shapes are commonly characterized by standard parametrizations which, while having some theoretical motivation, are justified primarily on a phenomenological basis (i.e., they give a decent fit to the data and/or theory). By fitting observed $d\sigma/dx_F$ and $d\sigma/dp_T^2$ distributions with these functional forms, we are able to quantify their shapes as a small number (1-3) of independent[7] parameters.

x_F range	$d\sigma/dx_F$ (μb/nucleon)		
	π beam	K beam	p beam
$-0.1 - 0.0$	17 ± 8	< 53	< 54
$0.0 - 0.1$	47 ± 3	48 ± 7	50 ± 7
$0.1 - 0.2$	35 ± 2	38 ± 4	31 ± 4
$0.2 - 0.3$	21.9 ± 1.4	24 ± 3	16 ± 3
$0.3 - 0.4$	11.4 ± 1.1	12 ± 2	3.5 ± 1.6
$0.4 - 0.5$	4.7 ± 0.8	5.2 ± 1.8	< 0.7
$0.5 - 0.6$	2.3 ± 0.6	4.2 ± 1.7	
$0.6 - 0.7$	1.1 ± 0.5	< 1.6	
$0.7 - 0.8$	< 1.1		

Table 9.1: E769 measurements of differential cross-sections vs. x_F for π, K, and p-induced D meson (D^+, D^-, D^0, $\overline{D}^0$, D_s^+, and D_s^-) production. In addition to the statistical errors shown, there are overall normalization errors of about 6%, 6%, and 9% for π, K, and p results, respectively. Inequalities are given for 90% confidence level upper limits.

[7]While the shape parameters are independent of one another, in general their errors, derived statistically using the fitter's minimization algorithm, are to some degree correlated.

p_T^2 range (GeV^2)	$d\sigma/dp_T^2$ (μb/(nucleon GeV^2))		
	π beam	K beam	p beam
$0-1$	8.3 ± 0.4	8.8 ± 0.8	6.2 ± 0.8
$1-2$	2.25 ± 0.16	2.6 ± 0.4	2.6 ± 0.4
$2-3$	0.90 ± 0.09	1.0 ± 0.2	0.69 ± 0.17
$3-4$	0.45 ± 0.06	0.56 ± 0.14	0.24 ± 0.10
$4-5$	0.28 ± 0.04	—	0.16 ± 0.07
$4-6$	—	0.07 ± 0.04	—
$5-6$	0.08 ± 0.02	—	0.11 ± 0.06
$6-7$	0.07 ± 0.02	—	—
$6-8$	—	0.06 ± 0.03	0.05 ± 0.03
$7-8$	0.025 ± 0.013	—	—
$8-10$	0.019 ± 0.007	< 0.02	< 0.02
$10-12$	0.006 ± 0.005		
$12-14$	0.007 ± 0.004		
$14-16$	< 0.005		

Table 9.2: E769 measurements of differential cross-sections vs. p_T^2 for π, K, and p-induced D meson (D^+, D^-, D^0, $\overline{D}^0$, D_s^+, and D_s^-) production. Description in Table 9.1 caption applies.

Theoretically-predicted $d\sigma/dx_F$ distributions, both for charm quarks (NLO QCD) and charm mesons (Lund MC), are well-fit in the x_F range accessible to E769 ($-0.1 < x_F < 0.8$) by the 3-parameter function defined in Equation 2.7. The former fits, described in Section 2.6.2, are used later in this section to compare measurements with theory; the latter fits determine the differential distribution correction functions (see Section 7.2.3) used to weight the MC in the absolute cross-section analysis. In fitting measured $d\sigma/dx_F$ distributions in the forward hemisphere, however, the following standard 1-parameter function (hereafter called the "n-form") is sufficient:

$$\frac{d\sigma}{dx_F} = N\ (1 - |x_F|)^n. \tag{9.9}$$

Although the data presented here does give some limited indication of the behavior

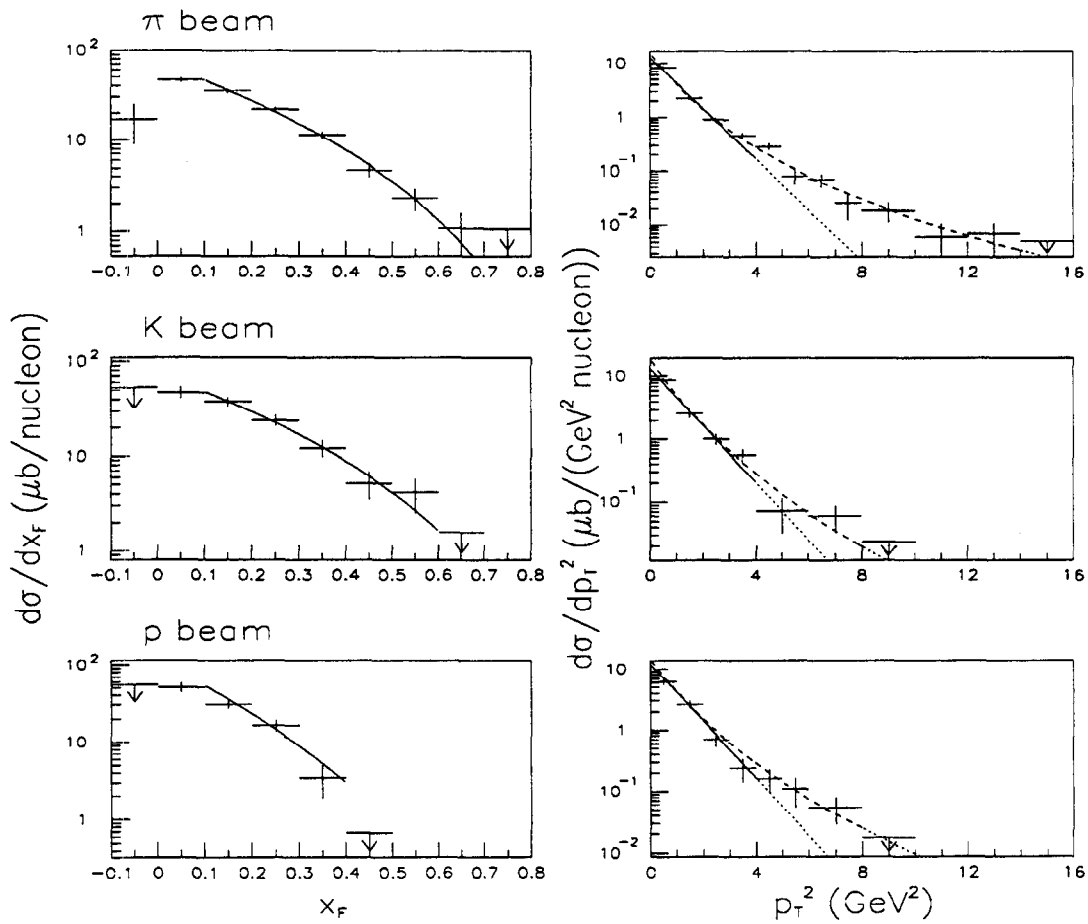

Figure 9.1: Combined D differential cross-sections with parametrization fits. Versus x_F (p_T^2), n-form (b-form) fits are indicated by a solid line. Fits of $d\sigma/dp_T^2$ using the FMNR form are shown as a dashed line. Extrapolations of fits beyond the fit range used are indicated by dotted lines.

of the cross-section in the backward hemisphere, negative-x_F cross-sections are not measured with enough precision to yield significant information about the "central" shape parameters x_c and x_b (defined in text following Equation 2.7). Use of the form of Equation 9.9 assumes, contrary to expectation in the case of π-induced production, that $d\sigma/dx_F$ is symmetric about zero. Furthermore, this function's discontinuous derivative at zero x_F gives it an unphysical cusp. Nevertheless, as stated above,

the shapes of measured $d\sigma/dx_F$ distributions in the full forward hemisphere can be characterized by the single "tail" parameter n. The usefulness of this parametrization is discussed further when results of the fits to data are presented later in this section.

Versus p_T^2, the 2-parameter FMNR form

$$\frac{d\sigma}{dp_T^2} = N\ (\alpha m_c^2 + p_T^2)^{-\beta}, \tag{9.10}$$

where m_c is the mass of the charm quark (set to 1.5 GeV), gives good fits to data (as well as theory) over the full p_T^2 range over which D meson signals are obtained (0-16 GeV^2). For the more precisely-measured distributions, this form supplants the following two forms, which provide acceptable fits to the data only at low and high p_T^2, respectively:

$$\frac{d\sigma}{dp_T^2} = N\ \exp -bp_T^2 \tag{9.11}$$

$$\frac{d\sigma}{dp_T^2} = N'\ \exp -b'\sqrt{p_T^2} = N'\ \exp -b'p_T. \tag{9.12}$$

The first exponential (b-form) is found to give poor-quality fits to the more precisely-measured distributions, even given the limited range in which it is used (0-4 GeV^2, unless otherwise specified). Unlike the FMNR function, however, the b-form has been used by numerous experimental collaborations to parametrize their results. The second exponential (b'-form) is found to give good fits to the data in the full range above p_T of 1 GeV.

In Figs. 9.1 through 9.6, we present plots of $d\sigma/dx_F$ and $d\sigma/dp_T^2$ for the combined D as well as the individual D meson species. Distributions for π, K, and p beams are each shown except in cases where the data is too scarce to break up into bins. As with the forward cross-sections (see discussion in Section 8.3.2), combined π and K beam results are used in comparisons with previous measurements made using negative meson beams. In Section 9.3.2, positive and negative π and K beam results are compared.

In the aforementioned plots, least-squares fits to $d\sigma/dx_F$ and $d\sigma/dp_T^2$ are also shown. The former distributions are fit using the n-form; although this form can be

Beam	x_F range	n	χ^2/dof	C.L.[a] (%)
π	> 0.1	4.4 ± 0.2	0.5	76
	> 0.0	4.03 ± 0.18	1.5	19
K	> 0.1	4.2 ± 0.5	0.4	72
	> 0.0	3.8 ± 0.4	0.7	57
p	> 0.1	7.1 ± 1.1	2.3	13
	> 0.0	6.1 ± 0.7	2.0	13

[a]confidence level (χ^2 upper-tail probability).

Table 9.3: Combined D $d\sigma/dx_F$ fit results.

Beam	p_T^2 range (GeV^2)	b (GeV^{-2})	χ^2/dof	C.L. (%)
π	0 - 4	1.08 ± 0.05	6.8	0.1
K	0 - 4	1.05 ± 0.09	1.7	18
	> 0	1.04 ± 0.08	1.7	15
p	0 - 4	1.08 ± 0.09	0.7	48
	> 0	0.99 ± 0.08	1.4	22

Table 9.4: Combined D $d\sigma/dp_T^2$ fit results, b-form.

used to fit $d\sigma/dx_F$ for all positive x_F, fits over the more limited range $x_F > 0.1$ are shown, primarily to follow the precedent set in earlier E769 differential cross-section papers [6, 9].[8] The p_T^2 distributions are fit using the b-form (solid line) in the p_T^2 range 0-4 GeV^2 and, in cases with data available beyond this range, the FMNR form (dashed line) over the full p_T^2 range. For both x_F and p_T^2 fits, the fitting functions used integrate given parametrizations over the width of a bin rather than returning the value at the bin center. The fits are done using all bins (in the range appropriate to

[8]In [6], inclusion of the first positive x_F bin led to a poor n-form fit to the combined D data. The x_F range in [9] was kept the same to facilitate comparison of D^* results with those presented in [6].

Beam	α	β	χ^2/dof	C.L. (%)
π	1.4 ± 0.3	5.0 ± 0.6	1.1	35
K	2.4 ± 1.6	7.6 ± 3.7	1.5	22
p	2.2 ± 1.5	6.6 ± 3.3	1.2	33

Table 9.5: Combined D $d\sigma/dp_T^2$ fit results, FMNR form.

Beam	p_T range (GeV)	b' (GeV^{-1})	χ^2/dof	C.L. (%)
π	1.0 - 3.742	2.74 ± 0.09	1.4	19
	1.0 - 2.449	2.58 ± 0.10	2.1	10
	0.0 - 3.742	2.28 ± 0.04	6.5	0
K	1.0 - 2.828	3.0 ± 0.3	1.7	17
p	1.0 - 2.828	3.0 ± 0.3	0.6	64

Table 9.6: Combined D $d\sigma/dp_T^2$ fit results, b'-form.

the parametrization) which have at least a 2σ signal (or are bounded by two bins that do). Upper limits[9] are shown for those bins which do not satisfy the above criteria but are adjacent to ones that do. The numerical values of the shape parameters returned by the fitter and information about the quality of the fits are given in Tables 9.3 through 9.14.

In Fig. 9.2, combined D $d\sigma/dp_T^2$ fits using the b'-form are plotted. As can be seen from the unusual binning used, the independent variable is transformed from p_T^2 to p_T by simply taking the square roots of the bin edges and rebinning the histograms. The results of these fits are given in Table 9.6.

As mentioned in Section 9.2, the n and b parameters exhibit a systematic dependence on the fit range chosen. As shown by the combined D $d\sigma/dx_F$ fit results

[9]For empty bins, Poisson statistics are used to obtain the 90% C.L. upper limit (2.3 events divided by the acceptance); for the rest, this limit is calculated through a Bayesian integration of a Gaussian, as described in Section 8.3.1.

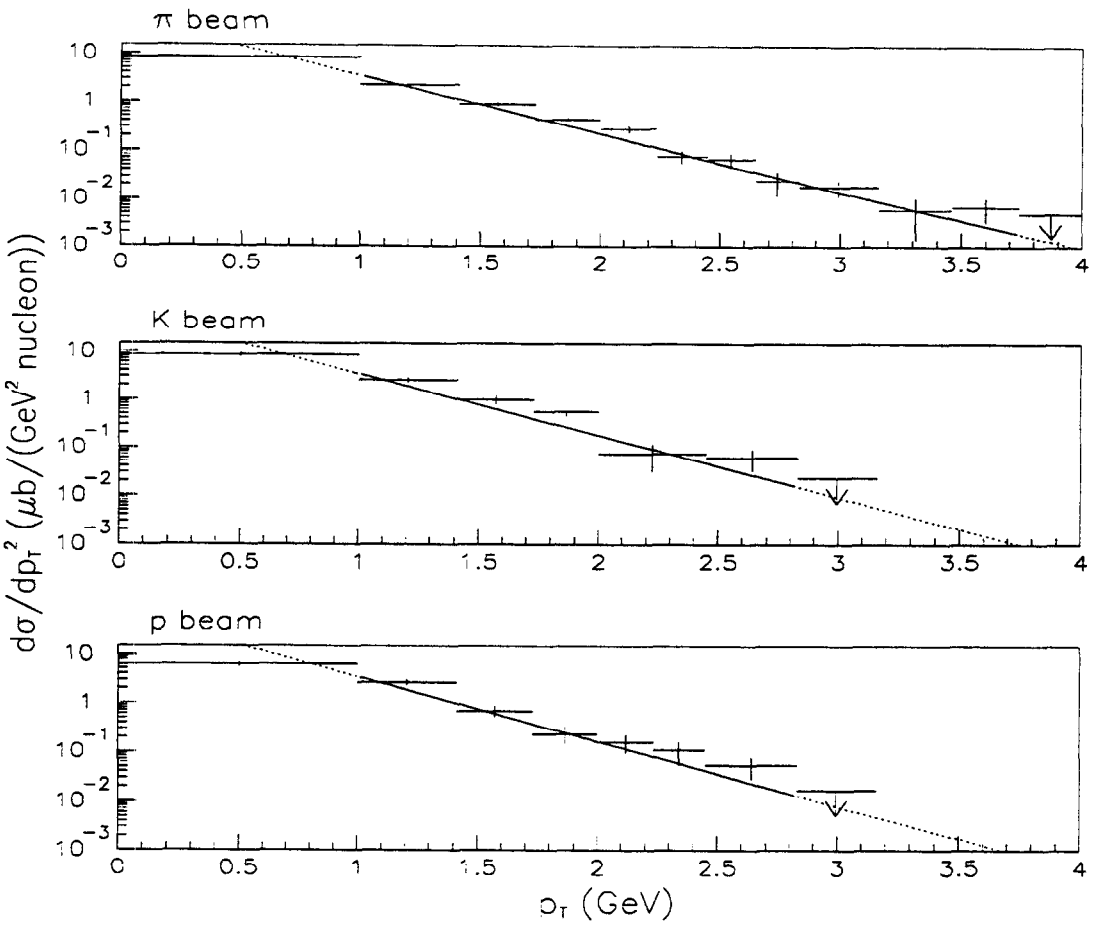

Figure 9.2: Combined D $d\sigma/dp_T^2$ (μb/GeV^2) vs. p_T (GeV). Fits using the b'-form are shown as a solid line. Extrapolations beyond the fit range used are indicated by dotted lines.

reported in Table 9.3, the inclusion of the 0.0-0.1 x_F bin in the fit decreases n it by 1-2σ. The use of the standard b-form to fit $d\sigma/dp_T^2$ is also problematic; as indicated by the good data fits obtained using the FMNR form, the cross-section dies out at high transverse momentum much more slowly than is consistent with exponential behavior in p_T^2. Therefore, data fits using the b-form are poor for the well-measured distributions. Even when the b-form fits the data acceptably, b decreases systematically as more of the high-p_T^2 tail is included in the fit range.

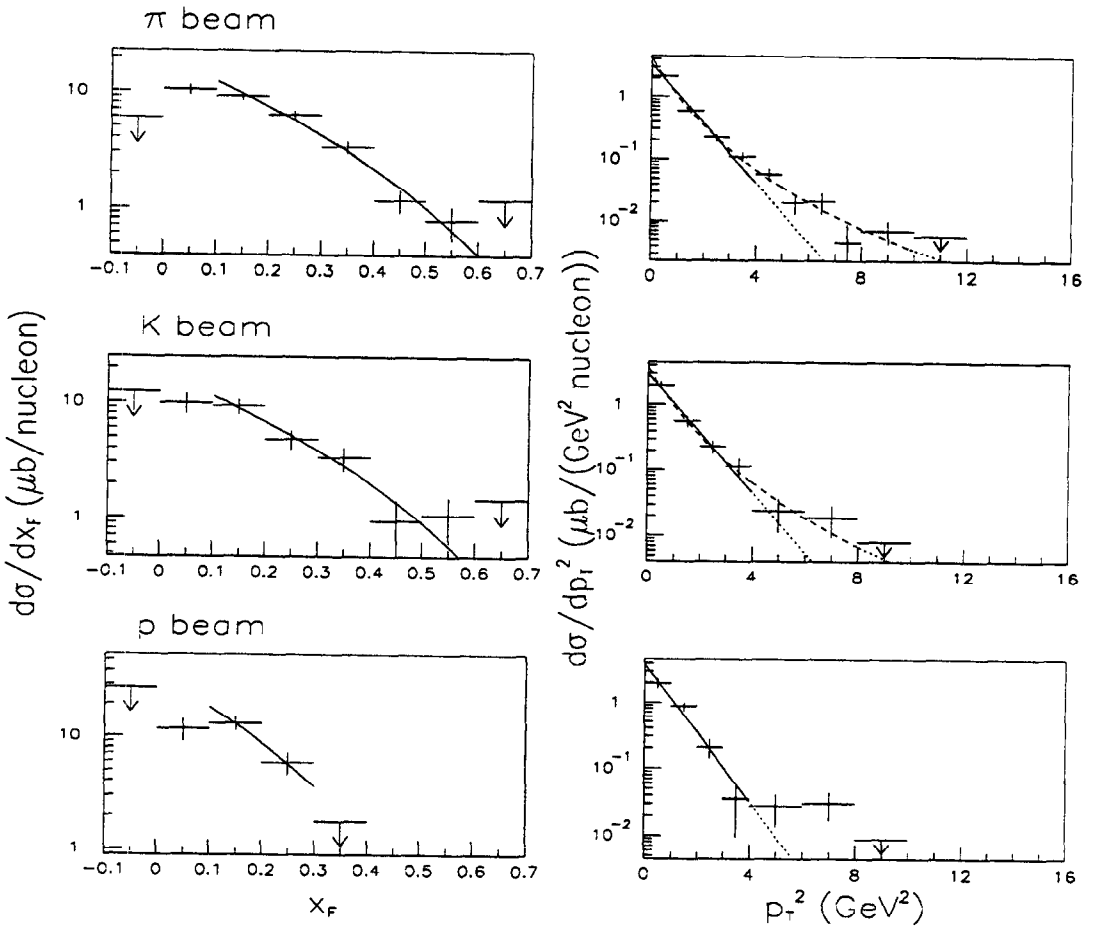

Figure 9.3: D^+ differential cross-sections. See Fig. 9.1 caption.

With these caveats in mind, we can make comparisons to previous measurements of differential cross-section shapes by comparing the standard n and b shape parameters. The FMNR form has not previously been used to fit data, and only E769 has reported b' values (see below). Previous measurements of combined D[10] (D^*) shape parameters are given in Tables 9.15 through 9.17 (Table 9.18). Note the different ranges in x_F and p_T^2 used by the various experiments as well as the changes in beam energy. Theory

[10]The combined D sample used by other experiments and in earlier E769 analyses does not include D_s.

Beam	n	χ^2/dof	C.L. (%)
π	4.2 ± 0.3	1.5	22
K	4.3 ± 0.7	.8	48
p	6.6 ± 2.1	—	—

Table 9.7: D^+ $d\sigma/dx_F$ fit results.

Beam	b (GeV^{-2})	χ^2/dof	C.L. (%)	α	β	χ^2/dof	C.L. (%)
π	1.10 ± 0.06	3.5	3	1.3 ± 0.4	4.7 ± 0.9	0.7	66
K	1.05 ± 0.12	0.9	40	1.4 ± 1.2	5.0 ± 2.9	0.6	64
p	1.19 ± 0.11	1.8	17				

Table 9.8: D^+ $d\sigma/dp_T^2$ fit results.

predicts that as beam energy rises from 200 to 800 GeV, n should rise by about 45% (30%) for $\pi(p)$-N charm production; over the same range in beam energy, b is expected to drop by about 20% (25%) [26].

For π, K, and p beams, the n and b results of the present analysis are largely consistent with previous measurements (including those of E769). Although for π-induced D production, the published b values tend to be significantly lower than those of E769, this can probably be attributed to the much larger p_T^2 ranges used in determining the former. In addition, the present analysis has not led to a significant change in the b' value obtained previously by E769 [6] for π-induced D production: 2.76 ± 0.08 GeV^{-1}, over a p_T range very similar to that used in this analysis. Not enough precise measurements are available to assess the accuracy of the energy dependence of the differential cross-section shapes predicted (for quarks) by perturbative QCD. The magnitudes of n and b expected from theory, however, are consistent with the trend in the data. At E769's beam energy, n is predicted to be about 4 (6.5) for

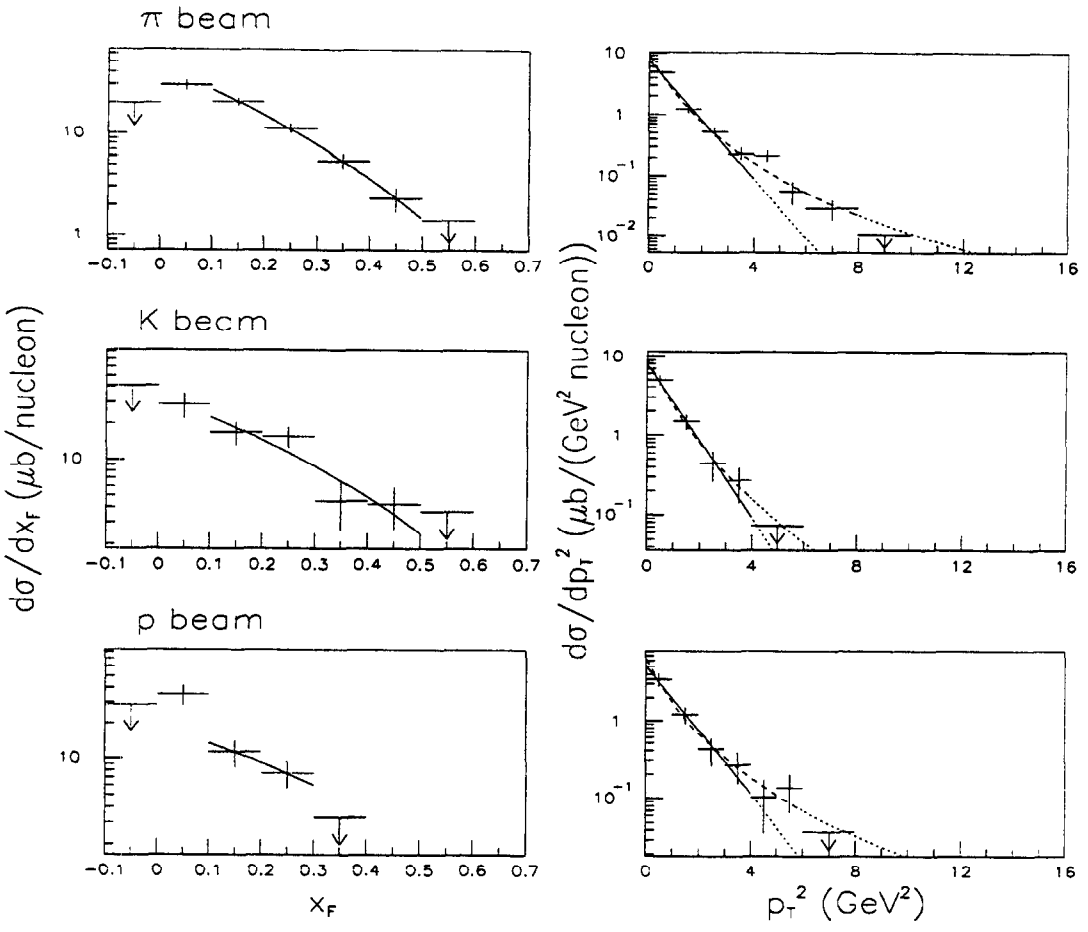

Figure 9.4: D^0 differential cross-sections. See Fig. 9.1 caption.

$\pi(p)$-induced production; b is predicted to be close to 1 GeV^{-2} in both cases [26].

As detailed in Section 2.6, NLO QCD predictions of the shapes of charm quark differential cross-sections (versus x_F and p_T^2) are generated for both π and p beam using the program of Mangano *et al.*; good fits to these distributions are obtained. Fits of the combined D measured distributions to theory, with the normalization kept floating, are carried out as parametrization-independent tests of the agreement between theory and data. The results of these fits are given in Tables 9.19 and 9.20.

Remarkably, D meson $d\sigma/dx_F$ distributions induced by π and p beams are well-fit

Beam	n	χ^2/dof	C.L. (%)
π	4.9 ± 0.5	0.03	97
K	3.8 ± 1.0	1.7	18
p	3.2 ± 2.9	—	—

Table 9.9: D^0 $d\sigma/dx_F$ fit results.

Beam	b (GeV^{-2})	χ^2/dof	C.L. (%)	α	β	χ^2/dof	C.L. (%)
π	1.11 ± 0.08	3.0	5	1.0 ± 0.4	4.0 ± 0.9	1.2	29
K	1.12 ± 0.16	0.4	66	1.4 ± 2.9	4.9 ± 7.3	0.3	56
p	0.96 ± 0.16	0.4	70	0.9 ± 1.1	3.3 ± 2.3	0.4	79

Table 9.10: D^0 $d\sigma/dp_T^2$ fit results.

by the corresponding predictions for charm quarks. These latter shapes are found to be insensitive to variation of parameters typically used to gauge theoretical uncertainty (m_c, μ_R, μ_F) [32, 37]. Furthermore, the π and p beam predictions for $d\sigma/dx_F$ are quite distinct, the former being significantly harder and peaking at 0.03 rather than being symmetric about x_F of zero. Consequently, the precision of the data is more than sufficient for the expected difference in π and p-induced production to be measured; the shape of the π (p) beam distribution is inconsistent with that of the p (π) beam theory. The K beam data is well-fit by the π beam theory, indicating similarity in pion and kaon gluon distributions.

The predicted separation between π and p-induced charm production is not as pronounced for $d\sigma/dp_T^2$ as it is for $d\sigma/dx_F$; the π beam distribution is expected to be somewhat harder. These shapes, further, show a dependence on moderate variations in m_c ($\pm$ 0.3 GeV) which is similar for both beams and on the order of the difference between them (see Section 2.6). The K and p beam shapes are fit well by either

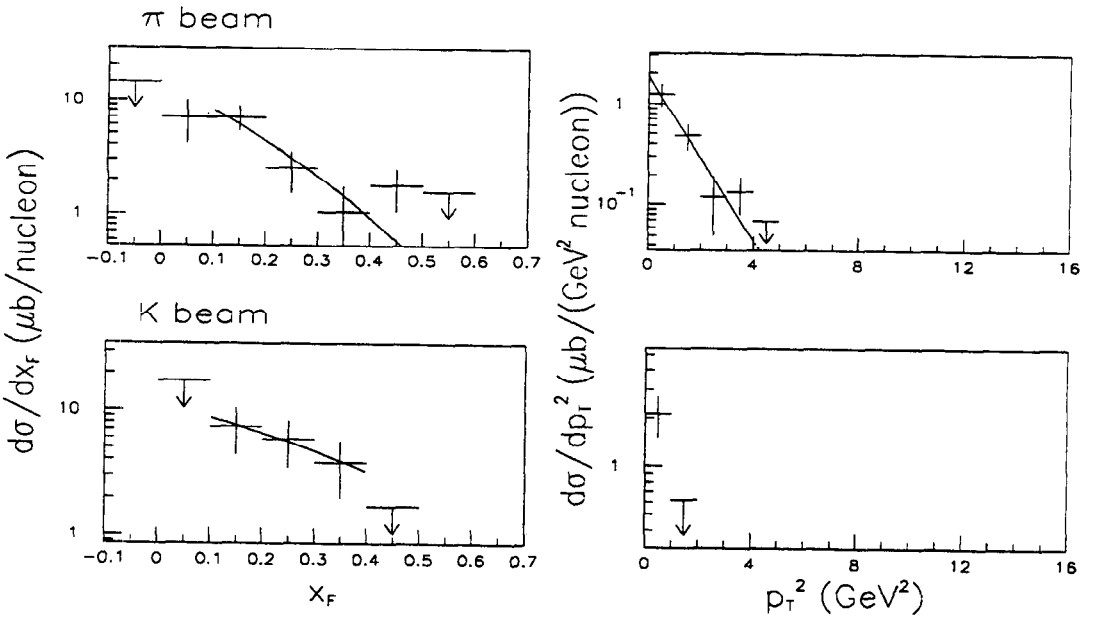

Figure 9.5: D_s differential cross-sections. See Fig. 9.1 caption.

Beam	n	χ^2/dof	C.L. (%)
π	5.3 ± 2.2	1.9	16
K	2.5 ± 2.3	0.02	88

Table 9.11: D_s $d\sigma/dx_F$ fit results.

theory curve. The π beam data distribution, however, while fit well by the theoretical distribution generated using π parton distributions for the beam, is inconsistent with the p beam theory.

These $d\sigma/dx_F$ and $d\sigma/dp_T^2$ data-theory comparisons are plotted in Figs. 9.7 and 9.8, respectively. Normalizations of the π (p) beam theory curves are floated for best fit to the π (p) beam data. It should be emphasized that the theory curves shown are for charm *quarks*; no attempt has been made to modify these predictions to

Beam	b (GeV^{-2})	χ^2/dof	C.L. (%)
π	0.9 ± 0.2	1.1	32

Table 9.12: D_s $d\sigma/dp_T^2$ fit results.

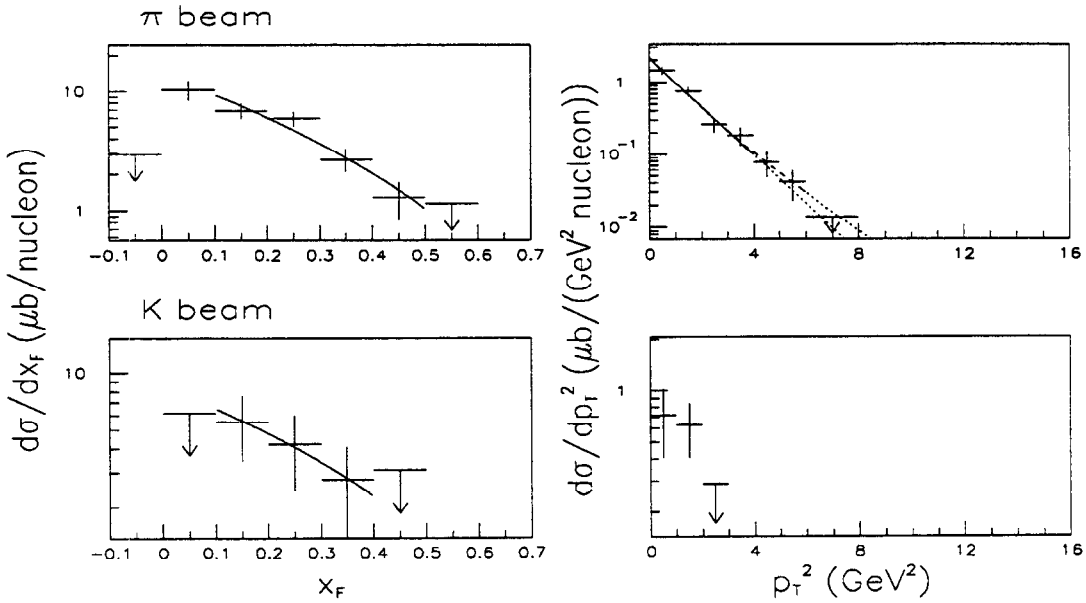

Figure 9.6: D^* differential cross-sections. See Fig. 9.1 caption.

incorporate non-perturbative effects such as intrinsic parton p_T and hadronization. At E769's level of precision, these corrections are evidently unimportant or fortuitously cancel out one another.

9.3.2 Beam particle dependence

As with the absolute cross-section results, we combine oppositely-signed π and K beam samples to obtain our most precise measures of the differential distributions

Beam	n	χ^2/dof	C.L. (%)
π	3.8 ± 0.6	1.3	28
K	2.6 ± 2.3	0.01	92

Table 9.13: D^* $d\sigma/dx_F$ fit results.

Beam	b (GeV^{-2})	χ^2/dof	C.L. (%)	α	β	χ^2/dof	C.L. (%)
π	0.77 ± 0.09	0.8	45	7.4 ± 9.3	14.0 ± 15.6	0.5	67

Table 9.14: D^* $d\sigma/dp_T^2$ fit results.

for the three E769 beam species (π, K, p). This procedure is supported by the arguments presented in Section 8.3.2. In fact, once issues of absolute normalization are ignored, dependence of the distribution shapes on beam particle charge should be further diluted because observed distributions are effectively averages of components which are not expected to be markedly dissimilar (e.g., gg fusion and $q\bar{q}$ annihilation). Results which support these assumptions are presented in this section.

By minimizing the χ^2 between two measured distributions (allowing the normalization of one of the distributions to float), we can obtain quantitative support (χ^2/dof, confidence level) for a statement concerning the (in)consistency of the shapes of the distributions. Of course, the range of the comparison is limited to that of the distribution measured with the lesser precision.

First, we carry out this procedure on the combined D differential distributions for oppositely-charged meson beams. Versus x_F, the π^-/π^+ (K^-/K^+) shape comparison fit returns a χ^2/dof of 1.7 (0.5), indicating consistency at the 14% (74%) confidence level. The evidence for consistency versus p_T^2 is slightly more compelling, with a $\chi^2/dof.$ of 1.0 (0.3) corresponding to a confidence level of 45% (79%). For each

Expt.	E_B (GeV)	# events	n (b (GeV^{-2}))	x_F range (p_T^2 range (GeV^2))
NA32	200	114	$2.5^{+0.4}_{-0.3}$	0.0 - 0.7
			$(1.06^{+0.12}_{-0.11})$	(0 - 5)
	230	792	$3.74 \pm 0.23 \pm 0.37$	0.0 - 0.8
			$(0.83 \pm 0.03 \pm 0.02)$	(0 - 10)
E769 (1992)	250	1307	3.9 ± 0.3	0.1 - 0.7
			(1.03 ± 0.06)	(0 - 4)
WA75	350	459	3.5 ± 0.5	-0.5 - 0.5
			(0.77 ± 0.04)	(0 - 10)
NA27	360	57	3.8 ± 0.63	0.0 - 0.9
			$(0.83^{+0.18}_{-0.16})$	(0 - 10)
E653	600	676	$4.25 \pm 0.24 \pm 0.23$	> 0.0
			$(0.76 \pm 0.03 \pm 0.03)$	

Table 9.15: Previous measurements of combined D shape parameters, π beam [17,19,6,16,2,29].

individual D species, these findings are corroborated by the consistency of the n and b shape parameters determined for oppositely-charged meson beams. In Fig. 9.9, combined D π^- and π^+ distributions are plotted together.

Next, we turn to the combined D $d\sigma/dx_F$ and $d\sigma/dp_T^2$ results for π, K, and p beams. As expected from the inability of the π (p) beam $d\sigma/dx_F$ theory curves to fit the p (π) beam data, these two data distributions are found to be inconsistent at a greater than 99% confidence level ($\chi^2/dof > 4$).[11] Versus p_T^2, the distributions for π and p beams are found to be consistent. (Recall, however, that this comparison is only conducted over the range of the less-precisely measured distribution, in this case that for p beam.) For both $d\sigma/dx_F$ and $d\sigma/dp_T^2$, K and π beam results are found to be consistent.

[11]The confidence level for *inconsistency* is just 100% minus the confidence level for consistency, previously defined.

Expt.	E_B (GeV)	# events	n (b (GeV^{-2}))	x_F range (p_T^2 range (GeV^2))
NA32	200	34	4.7 ± 0.9	0.0 - 0.6
			$(2.7^{+0.7}_{-0.5})$	(0 - 3)
	230	31	$3.56^{+1.08}_{-0.99} \pm 0.36$	> 0.0
			$(1.36^{+0.32}_{-0.26} \pm 0.04)$	

Table 9.16: Previous measurements of combined D shape parameters, K beam [17,19].

Expt.	E_B (GeV)	# events	n (b (GeV^{-2}))	x_F range (p_T^2 range (GeV^2))
NA32	200	9	$5.5^{+2.1}_{-1.8}$	> 0.0
			$(1.4^{+0.6}_{-0.4})$	
NA27	400	119	4.9 ± 0.5	0.0 - 0.6
			(0.99 ± 0.09)	(0 - 7)
E653	800	96	$6.8^{+2.1}_{-1.9}$	> 0.0
			$(0.84^{+0.10}_{-0.08})$	
E743	800	31	8.6 ± 2.0	0.0 - 0.5
			(0.8 ± 0.2)	(0 - 6)

Table 9.17: Previous measurements of combined D shape parameters, p beam [17,4,30,12].

9.3.3 Hadronization

In principle, we expect hadronization to impact the differential distributions through such non-perturbative effects as color-dragging and leading-particle enhancement. The latter is largely eliminated by combining particle and antiparticle signals together, although differences could persist between neutral-leading production and the average of leading and non-leading production. In addition, the fraction of a particular D meson species that is *directly* produced is relevant.

Expt.	E_B (GeV)	# events	n (b (GeV^{-2}))	x_F range (p_T^2 range (GeV^2))
NA32	200	46	$2.8^{+1.1}_{-0.9}$	0.0 - 0.7
			$(0.9^{+0.3}_{-0.2})$	(0 - 5)
	230	147	$3.14^{+0.40}_{-0.39}$	0.0 - 0.8
			(0.79 ± 0.07)	(0 - 10)
E769 (1994)	250	519	3.5 ± 0.3	0.1 - 0.6
			(0.70 ± 0.07)	(0 - 4)
NA27	360	8.5	$4.3^{+1.8}_{-1.5}$	0.0 - 0.5
			(0.9 ± 0.4)	(0 - 3)

Table 9.18: Previous measurements of D^* shape parameters, π beam [17,19,9,3].

Data	Theory	χ^2/dof	C.L. (%)
π	π	1.9	6
π ($x_F > 0$)		.9	49
K		.5	77
p		5.0	0.2
π	p	20.5	0.00
π ($x_F > 0$)		20.0	0.00
K		6.3	0.00
p		0.9	43

Table 9.19: Data fits to theory shapes, $d\sigma/dx_F$.

In the differential cross-section analysis, the assumption has been made that, for the pseudoscalar mesons D^+, D^0, and D_s, the *differences* in these effects are too small to be seen, given the precision of our shape measurements. (The high-quality fits of charm quark theory to the measured distributions supports a stronger assumption, namely that the sum total of hadronization as well as other non-perturbative effects is itself small.)

Data	Theory	χ^2/dof	C.L. (%)
π	π	1.4	18
K		1.7	14
p		0.9	53
π	p	2.8	0.2
K		1.0	43
p		1.2	33

Table 9.20: Data fits to theory shapes, $d\sigma/dp_T^2$.

The consistency check described in the previous section is also used to justify the combination of the D^+, D^0, and D_s meson distributions into combined D distributions. Using the π beam distributions, we find that the x_F (p_T^2) distributions for the pseudoscalar mesons are all consistent with one another at a 12% (47%) or greater confidence level ($\chi^2/dof < 2\,(1)$).

The issue of direct versus indirect production (Section 8.3.3) is addressed by comparing combined D and D^* results (π beam) for the differential cross-section shapes. Recall that only about 25% of the combined D sample is produced directly. The x_F distributions are found to be consistent at a 70% confidence level. Versus p_T^2, however, the shape comparison fit returns a χ^2/dof of 2.5, indicating inconsistency at a greater than 97% confidence level. It is evident upon comparison of the pseudoscalar and vector D values of b that the emission of a pion or photon leading to indirect D production significantly softens the transverse momentum spectrum (corresponding to a higher b value) with respect to that of the parent D^*. We calculate the magnitude of this effect for the pion emission case:

$$\begin{aligned} p_T^2(D^*) &= (\boldsymbol{p}_T(D) + \boldsymbol{p}_T(\pi)) \cdot (\boldsymbol{p}_T(D) + \boldsymbol{p}_T(\pi)) \\ &= p_T^2(D) + p_T^2(\pi) + 2\ \boldsymbol{p}_T(D) \cdot \boldsymbol{p}_T(\pi). \end{aligned} \tag{9.13}$$

The transverse components of momenta are invariant under boosts along the beam

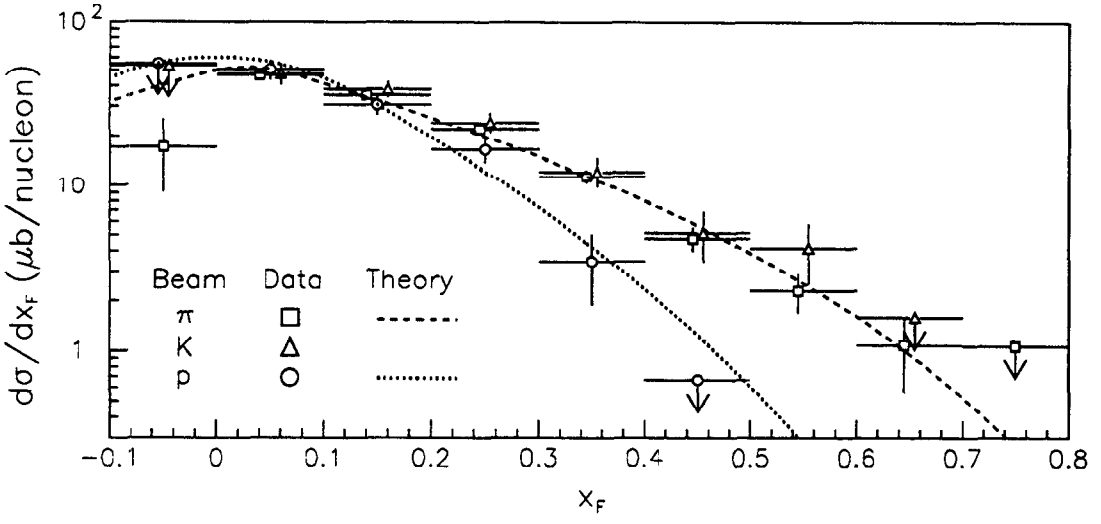

Figure 9.7: Measured D meson (D^+, D^-, D^0, $\overline{D}^0$, D_s^+, and D_s^-) $d\sigma/dx_F$ for production induced by π, K, and p beams and NLO QCD predictions [33] for charm quarks (π and p beams). In addition to the statistical errors shown, there are overall normalization errors of about 6%, 6%, and 9% for π, K, and p results, respectively. The abscissas of some data points are slightly offset to make them easily visible. Arrows indicate 90% confidence level upper limits.

axis; we choose to work in the frame where $p_L(D^*) = 0$. Within the transverse plane, we define the $x(y)$-axis as perpendicular (parallel) to the transverse momentum of the D^*. We now obtain an expression for the D^*-D difference in p_T^2:

$$\begin{aligned} \Delta &\equiv p_T^2(D^*) - p_T^2(D) \\ &= p_T^2(\pi) + 2\, \boldsymbol{p}_T(D) \cdot \boldsymbol{p}_T(\pi) \\ &= p_x^2(\pi) + p_y^2(\pi) + 2\, (p_x(D)\, p_x(\pi) + p_y(D)\, p_y(\pi)). \end{aligned} \tag{9.14}$$

Assuming that the D^* is produced on average with no net polarization, the D and π are produced back-to-back in the D^* rest frame with an isotropic angular distribution. Let ϕ and θ be the azimuthal and polar angles in this (primed) frame, respectively. In this frame, $p(D)' = p(\pi)' \equiv p_{CM} \simeq 36$ MeV, allowing us to express Δ as follows:

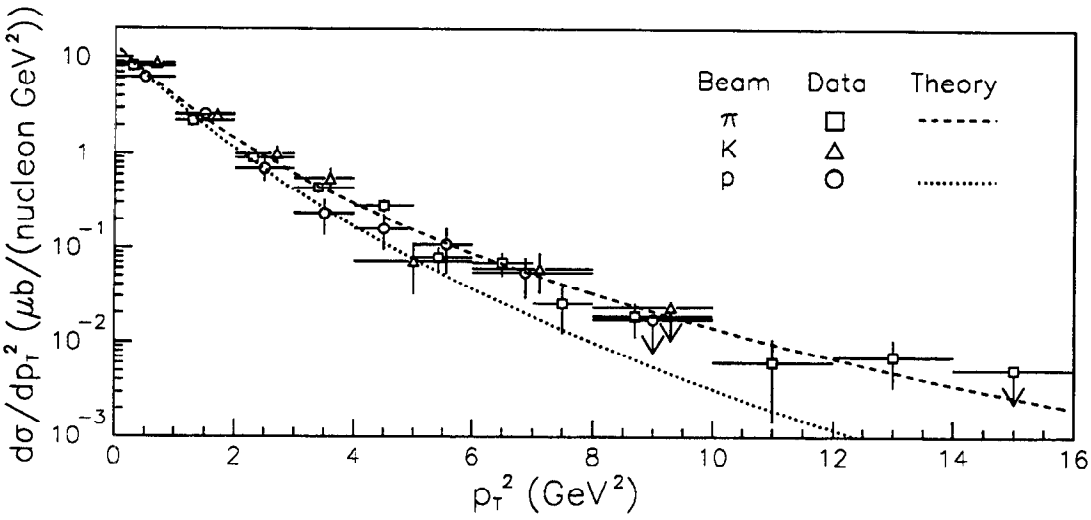

Figure 9.8: Measured D meson (D^+, D^-, D^0, $\overline{D}^0$, D_s^+, and D_s^-) $d\sigma/dp_T^2$ ($x_F > 0$) for production induced by π, K, and p beams and NLO QCD predictions [33] for charm quarks (π and p beams). See explanation in Fig. 9.7 caption.

$$
\begin{aligned}
\Delta &= p_x^2(\pi)' + \gamma^2 \left(p_y(\pi)' + \beta\, E(\pi)'\right)^2 + \\
&\quad 2\left(p_x(D)'\, p_x(\pi)' + \gamma^2 \left(p_y(D)' + \beta\, E(D)'\right)\left(p_y(\pi) + \beta\, E(\pi)'\right)\right) \\
&= p_{CM}^2 \cos^2\phi \sin^2\theta + \\
&\quad \gamma^2 \left(p_{CM}^2 \sin^2\phi \sin^2\theta - 2\beta\, p_{CM}\, E(\pi)' \sin\phi \sin\theta + \beta^2 E^2(\pi)'\right) - \\
&\quad 2\left[p_{CM}^2 \cos^2\phi \sin^2\theta + \gamma^2 \left(p_{CM}^2 \sin^2\phi \sin^2\theta + \right.\right. \\
&\quad \left.\left. \beta\, p_{CM} \left(E(D)' - E(\pi)'\right) \sin\phi \sin\theta - \beta^2 E(D)'\, E(\pi)'\right)\right], \qquad (9.15)
\end{aligned}
$$

where γ and β define the boost (in the transverse plane) from the D^* rest frame to our work frame.

Due to the low Q value of the D^* decay (5 MeV) with respect to the masses of the decay products, we can approximate the energies of the D and π in the primed frame with the masses of the respective particles. Averaging over the full solid angle, we obtain

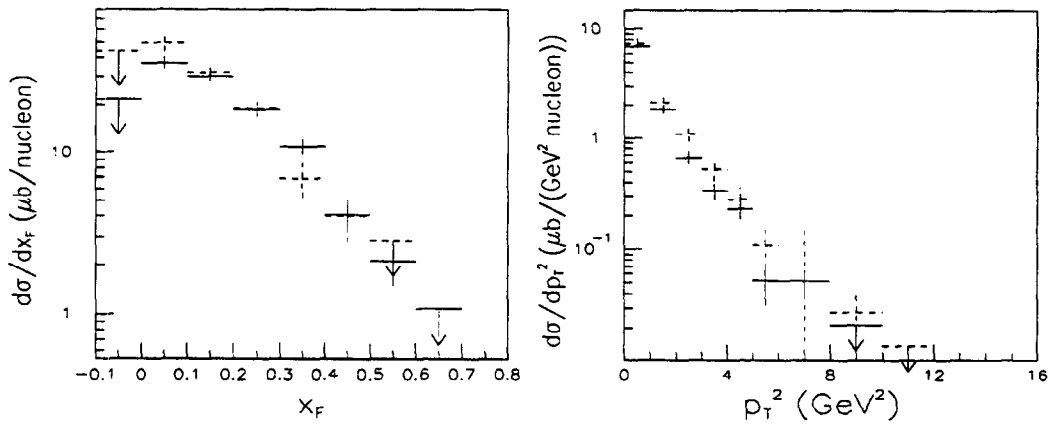

Figure 9.9: Combined D differential distributions compared for π^- (solid) and π^+ (dashed) beams. Left: $d\sigma/dx_F$ (μb/nucleon) vs. x_F, right: $d\sigma/dp_T^2$ (μb/(nucleon GeV^2)) vs. p_T^2 (GeV^2).

$$\begin{aligned}\Delta &= -\frac{p_{CM}^2}{3} + \gamma^2\left(\beta^2\left(2\,m_D + m_\pi\right)m_\pi - \frac{p_{CM}^2}{3}\right) \\ &= \frac{\beta^2}{1-\beta^2}\left[\left(2\,m_D + m_\pi\right)m_\pi - \frac{1}{3}\,p_{CM}^2\,\frac{2-\beta^2}{1-\beta^2}\right].\end{aligned} \tag{9.16}$$

Replacing β^2 with $p_T^2(D^*)/(m_{D^*}^2 + p_T^2(D^*))$, we obtain

$$\Delta = \frac{p_T^2(D^*)}{m_{D^*}^2}\left(\left(2\,m_D + m_\pi\right)m_\pi - \frac{1}{3}\,p_{CM}^2\right) - \frac{2}{3}\,p_{CM}^2. \tag{9.17}$$

Plugging in numerical values, we obtain

$$\Delta = 0.13 \times p_T^2(D^*) - 0.86\,\mathrm{MeV}^2. \tag{9.18}$$

Assuming that $p_T^2(D^*)$ has an exponential distribution, only the first term on the right-hand side of the equation impacts the relationship between the b values of the parent and daughter D mesons; this constant fractional change in p_T^2 leads immediately to a prediction that $b(D)$ be higher than $b(D^*)$ by about 15%, assuming there is no direct D production and all D^*'s decay to a pion and a D. The prediction for photon emission is obtained by replacing m_π by p_{CM} (~70 MeV in this case) in the

above equations; the effect is about half as large, leading to only a 7% increase in the average b value of the daughter D over that of the D^*.

Our π beam results provide the best measure of the b parameter ratio:

$$\frac{b(\text{combined } D)}{b(D^*)} = 1.40 \pm 0.18. \tag{9.19}$$

Although most D^*'s undergo $D\pi$ decays, we expect the effects derived above to be diluted somewhat by direct production of pseudoscalar D's ($\sim$25% of total). These considerations lead to an expectation that the combined D b value be higher than that of the D^* by 10-15%; our measured results are consistent with this prediction.